Pflugers Arch - Eur J Physiol (2014) 466:887–901
DOI 10.1007/s00424-013-1342-9

ION CHANNELS, RECEPTORS AND TRANSPORTERS

Ion transporters in brain endothelial cells that contribute to formation of brain interstitial fluid

Ruth Mokgokong · Shanshan Wang · Caroline J. Taylor · Margery A. Barrand · Stephen B. Hladky

Received: 7 August 2013 / Revised: 24 August 2013 / Accepted: 24 August 2013 / Published online: 11 September 2013

Abstract Ions and water transported across the endothelium lining the blood–brain barrier contribute to the fluid secreted into the brain and are important in maintaining appropriate volume and ionic composition of brain interstitial fluid. Changes in this secretion process may occur after stroke. The present study identifies at transcript and protein level ion transporters involved in the movement of key ions and examines how levels of certain of these alter following oxidative stress. Immunohistochemistry provides evidence for Cl^-/HCO_3^- exchanger, AE2, and Na^+, HCO_3^- cotransporters, NBCe1 and NBCn1, on brain microvessels. mRNA analysis by RT-PCR reveals expression of these transporters in cultured rat brain microvascular endothelial cells (both primary and immortalized GPNT cells) and also Na^+/H^+ exchangers, NHE1 (primary and immortalized) and NHE2 (primary cells only). Knock-down using siRNA in immortalized GPNT cells identifies AE2 as responsible for much of the Cl^-/HCO_3^- exchange following extracellular chloride removal and NHE1 as the transporter that accounts for most of the Na^+/H^+ exchange following intracellular acidification. Transcript levels of both AE2 and NHE1 are increased following hypoxia/reoxygenation. Further work is now required to determine the localization of the bicarbonate transporters to luminal or abluminal membranes of the endothelial cells as well as to identify and localize additional transport mechanisms that must exist for K^+ and Cl^-.

Keywords Rat brain endothelial cells · Blood–brain barrier · Brain interstitial fluid · Cl^-/HCO_3^- exchanger AE2 · Na^+, HCO_3^- cotransporters, NBCe1 and NBCn1 · Na^+/H^+ exchangers NHE1 and NHE2

Correct function of cells in the brain is dependent on the maintenance of suitable volume and ionic composition of the interstitial fluid (ISF) between the cells. This is determined by movement of ions and water in and out of cells, across the blood brain barrier and between ISF and cerebrospinal fluid (CSF). Water follows the osmotic gradients determined by the concentrations of the solutes, most importantly in the ISF, Na^+ and Cl^-. At steady state when the cells have constant composition, there is no net movement of ions into or out of them, and interstitial concentrations are thus determined by blood–brain transfer and exchanges with the CSF. Experiments where tracers are added have shown that both routes are important [21, 22, 55]. The transport of ions and water across endothelial cells forming the blood–brain barrier represents net secretion of fluid from blood to brain. This net secretion must be balanced by a net transfer of interstitial fluid out of the brain into the CSF, which is estimated to be between 10 and 30 % of the total rate of production

R. Mokgokong · S. Wang · M. A. Barrand · S. B. Hladky (✉)
Department of Pharmacology, University of Cambridge,
Cambridge CB2 1PD, UK
e-mail: sbh1@cam.ac.uk

C. J. Taylor
O'Brien Institute and Department of Surgery,
University of Melbourne, St. Vincent's Hospital,
42 Fitzroy Street, Fitzroy, Melbourne, VIC 3065, Australia

C. J. Taylor
Faculty of Health Sciences, Australian Catholic University,
Melbourne, VIC 3065, Australia

of CSF, with the remainder ascribed to the choroid plexuses [1, 15–17, 21, 46, 57, 74].[1]

Secretion of fluid by the blood–brain barrier must also be involved in local brain tissue swelling, i.e. focal oedema. Tissue volume increases must reflect either increased secretion or maintained secretion with decreased net rate of removal of fluid from the region to the CSF [67]. If there were to be changes in production or outflow of CSF, this would involve changes in fluid volume in spaces outside the brain parenchyma and so be associated primarily with hydrocephalus. Thus, to understand normal homeostasis of brain interstitial fluid and its failures, e.g. after ischaemic stroke with or without reperfusion, it is essential to understand the secretion process at the blood–brain barrier.

The mechanism of secretion of Na^+ and Cl^- across the endothelial cells that line the blood vessels forming the blood–brain barrier is known in broad outline (for a review, see [52]). Na^+ and Cl^- enter the endothelial cells largely via a Na^+, K^+, 2 Cl^- cotransporter, NKCC1, located in the luminal (blood facing) membrane [26, 54, 72], while the Na^+ leaves these cells largely via the Na^+, K^+–ATPase, the Na^+ pump, located in the abluminal (brain facing) membrane [5, 6, 25, 26, 48, 65]. The exit route for Cl^- is unknown: possibilities include anion channels and K^+, Cl^- cotransporters.

For HCO_3^- the major evidence for its mechanism of transport is the demonstration in cultured rat brain endothelial cells that under ambient conditions there is both Na^+, HCO_3^- cotransport that alkalinizes the cells and Na^+-independent Cl^-/HCO_3^- exchange that acidifies the cells, these occurring at comparable rates for intracellular pH (pH_i) near 7.1 [49, 76]. Thus, if Na^+, HCO_3^- cotransport were to be primarily at the luminal, blood-facing, membrane and the Cl^-/HCO_3^- exchange at the abluminal, brain-facing, membrane, then there would be net secretion of HCO_3^- into the brain. Combined activity of carbonic anhydrase [27, 76] with Na^+/H^+ exchange produces the same result as Na^+, HCO_3^- cotransport, but at pH_i above 7 the rate would be much less [49, 76]. Only at lower pH_i, e.g. 6.5, does Na^+/H^+ exchange become dominant [49].

The molecular identities of the transporters likely to move HCO_3^- at the blood–brain barrier have not so far been determined. Brain endothelial cells are known to express appropriate DIDS-sensitive SLC4A transporters. The cells also express NHE1 and NHE2 whose properties are suitable for the Na^+/H^+ exchange [41, 68, 76].

The present study identifies at transcript and protein level the ion transporters that could account for some of the activities observed. Immunohistochemistry provides clear evidence for AE2 and indications for NBCn1 and NBCe1 in the microvessels. Results from knock-down experiments using siRNA in cells of the GPNT brain endothelial cell line indicate that AE2 is responsible for the major part of the Cl^-/HCO_3^- exchange observed when Cl^- is removed from the external solution and that NHE1 accounts for most of the Na^+/H^+ exchange observed following intracellular acidification. Both AE2 and NHE1 transcripts are shown to be upregulated following hypoxia/reoxygenation.

Methods

Immunohistochemistry

Paraffin-embedded tissue Brain and kidney were fixed by perfusion of halothane-anaesthetized animals via the abdominal aorta with 4 % paraformaldehyde in 0.1 M cacodylate buffer, pH 7.4, according to the protocol of Praetorius [58]. Each organ was then cut into two equal halves, dehydrated using increasing concentrations of ethanol, embedded in paraffin and cut into 2 μM sections using a rotary microtome (Leica, Heidelberg, Germany). Sections were incubated in xylene overnight before staining. Initial rehydration was carried out by exposing slides to decreasing concentrations of ethanol. Endogenous peroxidase activity was blocked by 30 min of incubation in 0.5 % H_2O_2 in absolute methanol. Some sections were exposed to 0.1 % sodium dodecyl sulphate for 30 min prior to antigen retrieval that involved boiling in 1 mM Tris, pH 9, supplemented with 0.5 mM EGTA for 13 min. Non-specific binding was limited by exposure to 50 mM NH_4Cl and blockade in phosphate-buffered saline (PBS) supplemented with 1 % bovine serum albumin (BSA), 0.05 % saponin and 0.2 % gelatine. Sections were incubated at room temperature for 2 h, with the primary antibodies diluted in PBS supplemented with 0.1 % BSA and 0.3 % Triton-X-100, and after washing incubated with horseradish peroxidase conjugated goat anti-rabbit or goat anti-mouse IgG (Dako, Denmark) diluted in the same buffer. The peroxidase stain was developed using 0.05 % 3,3′-diaminobenzidine tetrahydrochloride (DAB) dissolved in PBS with 0.1 % H_2O_2. Mayers haemotoxylin was used as a counterstain. Tissue sections were dehydrated and mounted in hydrophobic Eukitt mounting medium (O. Kindler, Freiburg, Germany). Microscopy was performed on a Leica DMRE bright-field microscope equipped with a Leica DM300 digital camera.

[1] The mechanisms by which ions and water exchange between ISF and CSF have not been fully established. When viewed over distances less than a few hundred microns, movements of solutes and water within the ISF appear as diffusion (for reviews, see [21] and [73]). Viewed over larger distances, there is a superimposed, convective component, which can occur both towards and away from CSF and is primarily localized to the perivascular spaces surrounding blood vessels larger than capillaries [1, 15–17, 32, 33]. The uncertainty concerns the relative importance of convection and whether or not there is continuous circulation of fluid and solutes across the outer surfaces of the brain from CSF into ISF and back to CSF [1, 32, 33]. Such circulation may be very important for the delivery of intrathecally administered drugs to within diffusion distance of their targets (see e.g. [30]) but does not alter the need for a net efflux of ions and water to CSF to balance secretion across the blood–brain barrier.

Frozen tissue Whole rat brains were 'snap'-frozen in isopentane at −18 °C on dry ice and stored at −80 °C. Twenty-micrometre sections cut on a cryostat were thaw-mounted onto Vectabond™ (Vector Laboratories) coated slides, fixed in methanol at −20 °C for 2 min, and rehydrated in Tris-buffered saline (TBS, 50 mM Tris–HCl, pH 7.6, 150 mM NaCl) containing 0.2 % (*v*/*v*) Tween20 (TBS/Tween), and non-specific binding sites were blocked with 50 μg ml^{-1} BSA in TBS/Tween before application of the first primary antibody in blocking solution for 1 h at room temperature. Control slides were exposed for the same length of time but to blocking solution alone. Slides were then washed well and treated for 1 h at room temperature with the secondary antibody mixture containing Alexa Fluor™ 488 goat highly cross-absorbed anti-mouse IgG (H+L) conjugate at 1:50 (40 μg/mL) and Alexa Fluor™ 594 goat highly cross-absorbed anti-rabbit IgG (H+L) conjugate at 1:150 (13.33 μg/mL) (Molecular Probes, Portland, OR, USA). Sections were then washed well and mounted in glycerol/PBS (9:1 *v*/*v*) containing an anti-fading agent (DABCO at 2.5 mg ml^{-1}) and visualised by fluorescence microscopy.

An SDS epitope unmasking procedure was carried out for detection of both AE1 and AE2 [11]. Without this treatment, SA6 antibody stains mainly AE1, whereas the antibody reacts with both AE1 and AE2 following epitope unmasking. Briefly, the procedure involves fixing the sections in a solution containing 4 g paraformaldehyde, 2.739 g L-lysine and 0.428 g sodium metaperiodate in 200 ml phosphate buffer, pH 7.4, for 30 min at room temperature or immersion-fixing overnight at 4 °C. The sections were then washed and rehydrated in PBS containing 0.2 % (*v*/*v*) Tween-20 and incubated with 10 mg ml^{-1} sodium dodecyl sulphate in the same buffer for 4 min before treatment with primary and secondary antibodies as described earlier. Previous studies using this method have allowed immunolocalization of AE2 in basolateral membranes of several rat kidney tubular epithelial cell types [2] and on the basolateral membrane of epithelial cells in the initial segment and intermediate zone of the rat epididymis [35].

Sections were visualised by fluorescence microscopy, with light being provided either by a mercury arc lamp (Zeiss Axioskop) or a scanning confocal laser (Biorad Micro-Radiance). With the Bio-Rad system, sequential images were obtained (Kalman average of eight to ten individual scans) and the two parent images were merged using Lasersharp software.

Antibodies The antibodies used with thin sections cut from wax-embedded tissue are listed in Table 1. For the work with thick sections cut from frozen tissue, the same antibodies were used for AE2, AQP4 and NBCe1. Other antibodies used with thick sections are listed in Table 2.

Isolation of brain microvessels and endothelial cell culture

Microvessel fragments were isolated from rat brain tissue according to a method described previously [3, 63]. Endothelial cells were grown out from these microvessels in collagen-coated flasks and maintained in a medium containing Ham's F-10 medium with 10 % (*v*/*v*) foetal bovine serum (FBS), 75 μg/mL endothelial cell growth supplement (First Link, (UK), Ltd., Birmingham, UK), 80 μg/mL heparin, 5 μg/mL vitamin C, 2 mM L-glutamine, 100 U/ mL penicillin and 100 μg/mL streptomycin. Cells were used at passages 2–4.

The GPNT cell line [62] is an immortalised rat brain endothelial cell line derived from the GP8 cell line [29]. Cells used in this study were a kind gift from Dr. I. Romero (Open University, Milton Keynes, UK). Cells were maintained on collagen-coated flasks in a 1:1 mix of Ham's F-10: MEM-α supplemented with 10 % (*v*/*v*) FBS, 2 mM L-glutamine, 100 U/mL penicillin, 100 μg/mL streptomycin, 2 μg/ mL basic fibroblast growth factor (First Link) and 5 μg/mL puromycin.

Application of oxidative challenge

Cells grown to confluency in multiwell plates were exposed to oxidative challenge in one of two ways as described in [63], either by direct application of medium containing 200 μM H_2O_2 to each well or by applying hypoxic conditions to cells for 6 h followed with reoxygenation as described [63]. For this latter method, cells were treated with medium that had been pre-bubbled with 95 % N_2 in CO_2 for 3 min and then placed in a hypoxia chamber (Bilups-Rothenburg, www.brincubator.com) flushed with a mixture of 95 % air/5 % CO_2 and 95 % N_2/5 % CO_2 and maintained at 1 % O_2 for 6 h. Cells were reoxygenated by feeding with fresh, fully oxygenated medium and were replaced into the incubator for the times indicated before analysis.

RT-PCR analysis and reference gene selection

Total cellular RNA was isolated using TriPure Isolation Reagent (Roche, Derbyshire, UK) and cDNA was generated by reverse transcription using random hexamers as described previously [63]. Fragments specific to the rat genes of interest were then amplified by PCR using SensiMix (Quantace Ltd, Watford, UK) containing SYBR green and the appropriate primer pairs (see Table 3). Reactions were run on Rotor-gene 3000 (Corbett Research, Sydney, NSW, Australia). Thermal cycling conditions included initial denaturation for 10 min at 95 °C followed by 45 cycles of 95 °C for 30 s, 55 °C for 30 s and 72 °C for 30 s, with terminal elongation being performed at 72 °C for 2 min with a melt curve analysis from 72 to 99 °C. Data were analysed using the comparative quantitation option in Rotor-gene 3000 software (Corbett Research). As identified by and described in Robertson et al. [63], the reference gene

Table 1 Antibodies used with thin sections (all were raised in rabbits)

Antibody	Source	Reference
NHE1	ADI	
AE2	Seth Alper, Harvard	Alper SL et al., 1997 [2]
rkNBC1 (Slc4a4, NBCe1)	Aarhus	Maunsbach AB et al., 2000 [45]
NBCn1 (Slc4a7)	Aarhus	Kwon TH et al., 2002 [40]
Vacuolar H^+–ATPase	Aarhus	Pushkin A et al., 1999b [61]
		Pushkin A et al., 2000 [60]
Na^+, K^+–ATPase	Aarhus	Kashgarian M et al., 1985 [37]
AQP1	Aarhus	Nielsen S et al., 1993 [51]
AQP4	Aarhus	Terris J et al., 1995 [77]
PECAM (CD31)	Chemicon	

most suitable for H_2O_2 exposure experiments was beta-actin and for hypoxia/reoxygenation it was hypoxanthine-guanine phosphoribosyltransferase.

Luciferase reporter gene assay

To detect the activation of NHE1 promoter, a construct (kindly donated by Dr. Katarzyna Kania, Polish Academy of Sciences, Lodz, Poland) containing a NHE1-specific gene promoter sequence inserted into the pGL4.10[luc2] vector was transfected by electroporation using the Amaxa endothelial transfection kit (Lonza, Basel, Switzerland). A vector encoding a secretable form of alkaline phosphatase (pCMV-SEAP) under the control of a cytomegalovirus-derived promoter was co-transfected as described in Robertson et al. [63]. Following electroporation, cells were divided between six and nine wells of 24-well plates and maintained in medium for 24 h before treatment with hypoxia/reoxygenation as described earlier. After the requisite treatment times, the medium was harvested for alkaline phosphatase activity and the cells were analysed for luciferase activity, with values being normalised to the alkaline phosphatase activity as described previously [63].

Use of siRNA targeted against AE2 or NHE1

siRNA transfection mixes were prepared as follows: 50 nM of the siRNA duplexes (Qiagen) (sequences shown below) was diluted in 100 μl Opti-MEM with gentle mixing, 3 μl of INTERFERin^{TM} (Polyplus transfection), then added to the solutions and allowed to incubate for 10 min. To apply to GPNT cells already grown to ~50 % confluency in 24 well plates, the growth medium was removed from each well and 0.5 ml fresh medium was added. A total of 100 μl of the siRNA mix was then added and the plate was incubated at 37 °C. For RNA, cells were harvested after 24 h, and for fluorimetry or immunocytochemistry cells were trypsinised after 48 h and plated on glass coverslips.

Two duplexes were targeted against AE2:

Sequence 1, sense r(GCG CCA ACA UGG ACU ACC A)dTdT and antisense r(UGG UAG UCC AUG UUG CGC C)dTdG

Sequence 2, sense r(GCC UAA CAC UGC CUU GCU A)dTdT and antisense e(UAG CAA GGC AGU GUU AGG C)dTdG

One duplex was targeted against NHE1:

Sequence 3, sense 5′CCGCAATTTGACCAACTTATA-3′ and antisense 5′-UAUAAGUUGGUCAAUUGCGC-3′

Table 2 Antibodies used with thick sections (the antibodies used against AE2, AQP4 and NBCe1 were the same as in Table 1)

Antibody	Raised in	Source	Reference
N1P1G (NHE1)	Rabbit	Josette Noel, Montreal	Granger D et al., 2003 [28]
mNCBE 1139AP	Rabbit	Aarhus	Praetorius J et al., 2004 [58]
ntNBCn1 2977AP	Rabbit	Aarhus	Damkier H et al., 2006 [19]
ntNBCe2 7249AP	Rabbit	Walter Boron, Yale via Aarhus	Bouzinova EV et al., 2005 [9]
NCBE	Rabbit	Aarhus	Praetorius J et al., 2006 [59]
NDCBE	Rabbit	Aarhus	Damkier HH et al., 2007 [20]
PECAM1	Mouse	Chemicon	
Alexa Fluor 594 Anti-rabbit IgG	Goat	Molecular Probes	
Alexa Fluor 488 Anti-mouse IgG	Goat	Molecular Probes	

Table 3 Primers for the detection of mRNA for the indicated rat transporters

Gene	Primer pair sequence	Accession number
Slc9a1, NHE1	5′-ATGTGGCTGGGAAACAAGAC-3′	NM_012652
	5′-AGTGGTCCTCATCACCCAA-3′	
Slc9a2, NHE2	5′-ACTGGGGTCACAACTTCTGG-3′	NM_012653
	5′-TCCCTGTCTCTGCCATCTCT-3′	
Slc9a3, NHE3	5′-ACAGAAGCGGAGGAATAGCA-3′	NM_012654
	5′-TATCAATTCCTGCCCCAGAG-3′	
Slc9a4, NHE4	5′-GGGAAGAACCATGAGTGGAA-3′	NM_173098
	5′-GGGAAAAGGGTCAGAGGAAG-3′	
Slc9a5, NHE5	5′-TGTCTTCTGACCCTCGCTCT-3′	NM_138858
	5′-TACAGCCTGCCTCCTCTGTT-3′	
Slc4a1, AE1	5′-GCTTCTGGCTTATCCTGCTG-3′	NM_012651
	5′-AGCGGGTAGTCCTGGAAAAT-3′	
Slc4a2, AE2	5′-GAGCCCTTCTGCTGAAACAC-3′	NM_017048
	5′-CGCTCTCTATCCACCTCCAG-3′	
Slc4a3, AE3	5′-AAAAGCCTGAAACTGCTGGA-3′	NM_017049
	5′-GCCCTAGCTCGTGATAGTCG-3′	
Slc4a4, NBCe1	5′-TAGCGACAACGACGATTCTG-3′	NM_053424
	5′-TTGAGGCACGACTTTCACTG-3′	
Slc4a5, NBCe2	5′-GTTCGTCTTGCCCAGTCTTC-3′	NM_212512
	5′-TCATCAACTCCTGCGATCAG-3′	
Slc4a7, NBCn1	5′-AAACATCACCACCGGAGAAG-3′	NM_058211
	5′-TCTTCGAACTTCAGCCACCT-3′	
Slc4a8, NDCBE	5′-ACGGGGATTGCCTACTCTCT-3′	NM_199497
	5′-AGTCGCCACCAGGACAATAC-3′	
Slc4a10, NCBE, NBCn2	5′-GGCATGTACCTCTCCGAAAA-3′	NM_178092
	5′-CATCGAGCCAGCTAAGTTCC-3′	
GAPDH	5′-AAACCCATCACCATCTTCCA-3′	NM_017008
	5′-GTGGTTCACACCCATCACAA-3′	
β actin	5′-TGTCACCAACTGGGACGATA-3′	NM_031144
	5′-AACACAGCCTGGATGGCTAC-3′	
HPRT	5′-CTCATGGACTGATTATGGACAGGAC-3′	NM_012583
	5′-GCAGGTCAGCAAAGAACTTATAGCC-3′	Jaulmes et al., 2006 [34]

HPRT hypoxanthine phosphoribosyltransferase

The All Stars (Alexfluor 488) scrambled siRNA sequence information is unavailable due to proprietary rights (Qiagen).

Functional studies

Na^+/H^+ and Cl^-/HCO_3^- exchange activities were inferred from measurements of intracellular pH, pH_i. This was measured as described in detail by Taylor et al. [76] using the fluorescent indicator 2′,7′-bis-(2-carboxyethyl)-5-(and-6)-carboxyfluorescein (BCECF) introduced into cells via exposure to membrane-permeant BCECF-AM. Fluorescence was excited alternately at a pH-insensitive wavelength 440 nm and a pH-sensitive wavelength 502 nm, and the pH was calculated from the ratio of the background-corrected emissions measured at 530 nm. A calibration curve for converting the ratio to pH was determined for rat brain endothelial cells using a combination of nigericin-high K^+ and weak acid/weak base null point methods [76].

Na^+/ H^+ exchange was assessed using an ammonium prepulse as described previously [49, 76]. Briefly, cells were exposed to 20 mM NH_4Cl, replacing the same amount of NaCl in the external Hepes-buffered solution (nominally HCO_3^- free) for 200 s followed by return to a fresh aliquot of the original solution. During the exposure, pH_i initially shifts rapidly to a more alkaline value corresponding to diffusion into the cells of NH_3 and its combination there with H^+ to form NH_4^+. pH_i then partly recovers, which, because the NH_3 concentration is then constant, implies a further increase in NH_4^+. When the cells are returned to NH_4Cl-free solution, all the NH_4^+ exits as NH_3, leaving behind H^+ that greatly reduces pH_i. In the nominal absence of HCO_3^-, recovery is virtually abolished by either replacement of external Na^+ with $NMDG^+$ or application

of 5 μM 5-(*N*-ethyl-*N*-isopropyl)amiloride (EIPA) [49, 76]. The NHE1 inhibitor, cariporide (HOE642), was made up within 3 h of use as a 100-mM stock in distilled water.

Cl^-/ HCO_3^- exchange was assessed from the increase in pH_i when external Cl^- was removed. This removal leads to a DIDS-inhibitable exchange of internal Cl^- for external HCO_3^- [76].

Results

Detection of transporters in rat brain

Immunohistochemical studies to detect the location of ion transporters in rat brain were initially carried out using a panel of antibodies selective for Na, K–ATPase, AE2, AQP4, AQP1, NHE1, NHE3, NBCe1 and NBCn1 as shown in Table 1. These were kindly supplied by Dr. Jeppe Praetorius. The techniques followed those published by Praetorius and collaborators and involved 2-μM sections cut from wax-embedded rat brain. These were able to detect the transporters concerned in choroid plexus or kidney, with examples shown for the first three in Fig. 1. However, with the exception of AQP4, which is known to be expressed at high levels in the astrocyte end-feet that surround the microvessels [50], none of the other antibodies produced detectable specific staining around the microvessels in the brain slices. An antibody against CD31, PECAM, which is known to be present in brain microvessels, also failed to produce detectable staining in the thin sections. It was concluded from this that though these techniques were appropriate for localizing transporters that are highly expressed, they were inadequate for detecting transporters that are expressed at lower levels as may be the case in or on the microvessel walls. Hence, these results indicated that the ion transporters of interest must be expressed in brain and the microvessels at levels lower than those found in the specialized transporting epithelia of choroid plexus and kidney.

To enhance the sensitivity of detection, immunohistochemistry using fluorescent secondary antibodies was applied to thicker sections cut from frozen blocks. The advantage of thicker sections is that a field of view will contain more transporters, allowing easier detection; the disadvantage is that spatial discrimination and resolution allowing structural features to be displayed are inevitably lost. It was however possible to locate blood vessels in the frozen sections using an anti-PECAM antibody. This is illustrated in Fig. 1f for anti-AQP4 and anti-PECAM antibodies raised in different species and hence detectable with different secondary antibodies. The fluorescence corresponding to the location of the AQP4 antibody (shown in red) is seen to surround that for the PECAM antibody (shown in green).

This approach was applied to detect AE2, NBCe1 and NBCn1 in frozen rat brain slices as shown in Fig. 2. To reveal the presence of AE2, it was necessary to use an unmasking procedure [11] before the application of the primary antibody as described in "Methods" and the figure legend. With unmasking, AE2 was seen to be distributed along the walls of the microvessels (Fig. 2c, d). The antibody used to detect AE2 also binds to AE1 within the red blood cells, which can be seen clearly with or without unmasking (Fig. 2a–d). With NBCn1, there is binding along the course of the vessels and also to other components in the brain, while with NBCe1 the same appears to occur but less clearly. Background staining with the secondary antibodies alone was minor, i.e. less than the diffuse staining seen in Fig. 2a, b. Immunohistochemistry provides evidence for the presence of AE2, NBCn1 and possibly NBCe1 on the microvasculature. No evidence was found using these methods for NBCe2, NCBE (NBCn2) or NDCBE protein along the microvessels consistent with either no expression or low expression comparable to that seen on the surrounding cells.

Evidence for ion transporter expression in cultured rat brain endothelial cells

In order to explore the possible functional significance of the ion transporters detected in the brain vascular endothelium, it was necessary to undertake experiments on primary cultured rat brain endothelial cells (RBECs) and on immortalized rat brain endothelial cells (GPNT cells). To ensure that these cells expressed the ion transporters detected in vivo, mRNA analyses were firstly carried out.

As previously reported [76] for RBECs, compared to that for NHE1, a relatively large amount of mRNA for AE2, ca. sixfold less for AE3 and ca 100-fold less for AE1 was found. Of the NBCs, NBCe1 and NBCn1 were most highly expressed, NCBE and NDCBE somewhat less and NBCe2 ca. 80-fold less. In a more recent study where AEs were compared in primary cultured RBECs and in cells of the immortalized GPNT line, there was found to be less AE3 (relative to NHE1 in the same cell type) but somewhat more AE2 than seen previously (see Fig. 3).

Expression of NHE 2–5 relative to NHE1 was also examined. Results are shown in Fig. 3 for RBECs and GPNT. NHE2 mRNA is approximately 50-fold less than that of NHE1 in the RBECs and at least 500-fold less prominent relative to NHE1 in the GPNT cell line. Primers were validated using whole rat brain and whole rat kidney. They detected NHE 2, 4 and 5 at more than 10 % of the level for NHE1 in whole rat brain and detected NHE3 at the same level as NHE1 in whole rat kidney.

Experiments were also performed to determine whether oxidative challenge might alter the expression of AE2 and NHE1 and the activity of the NHE1 promoter. For this purpose, GPNT cells were used, these being more readily amenable to transfection of the reporter gene construct. Oxidative

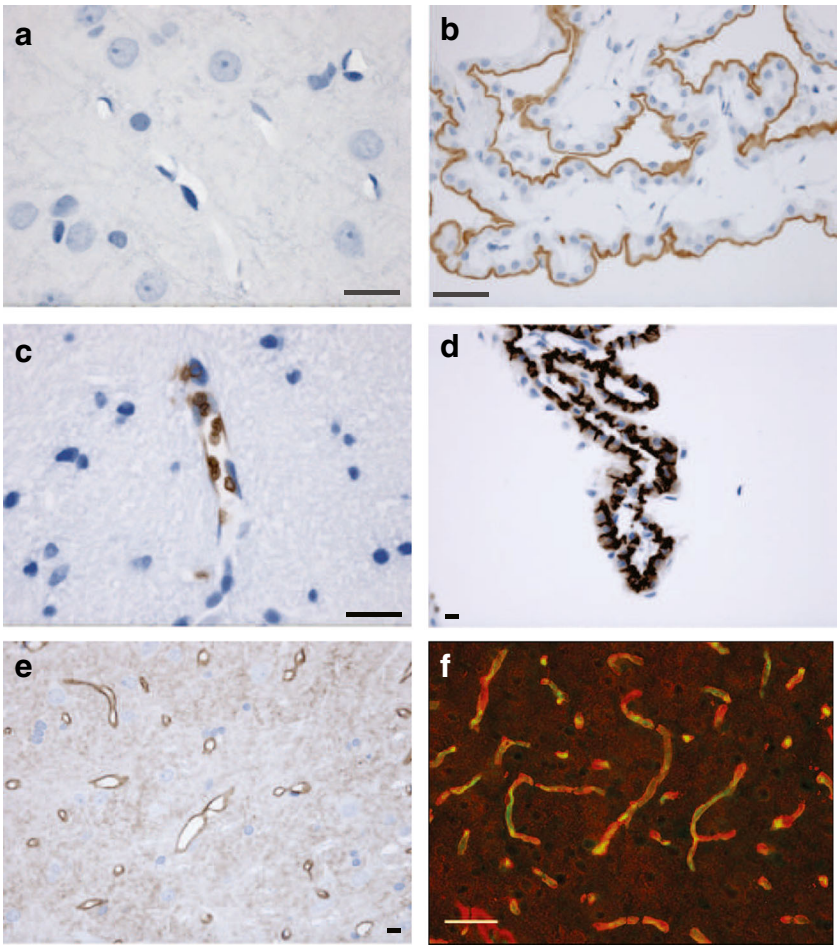

Fig. 1 Immunohistochemical detection of Na, K–ATPase, AE2, AQP4 and PECAM in rat brain. **a**, **c** and **e** Images obtained from 2-μm wax embedded sections of brain stained for Na, K–ATPase, AE2 and AQP4 using the techniques previously employed to detect these proteins in choroid plexus and kidney. The staining in **c** shows AE1 in red blood cells within a larger blood vessel. **b**, **d** Images that illustrate positive controls for Na, K–ATPase and AE2 in choroid plexus obtained in parallel experiments conducted at the same time with the same materials. Similarly, negative results for the microvessels and positive results for appropriate controls were obtained with antibodies for NHE1, NHE2, NHE3, AQP1, NBCe1 and NBCn1 (not shown). Only for AQP4 (shown in **e**) was there a clear specific staining surrounding small blood vessels in the thin brain sections. No staining was obtained in the thin sections with antibody for PECAM (also known as CD31). By contrast, in a ~20-μM frozen section from brain (**f**) stained for both PECAM (*green*) and AQP4 (*red*), a fluorescent signal for each is clearly evident following the course of the blood vessels. *Scale bars*: *black* 10 μM, *white* 50 μM

challenge was imposed by direct application of H_2O_2 or by exposing the cells to 6 h of hypoxia, 1 % O_2 and 5 % CO_2 in reduced serum medium, followed by 16 h of normoxia, 5 % CO_2 in air. As shown in Fig. 4, both types of challenge significantly increased the expression of mRNA for AE2 and NHE1. Furthermore, using a luciferase reporter gene construct, it was also shown that hypoxia/reoxygenation increased the activity of the NHE1 promoter.

Evidence for ion transporter activity in cultured rat brain endothelial cells

Having established the presence of mRNA for the above ion transporters in cultured rat brain endothelial cells, studies were undertaken to look for the functional activities of these transporters. Procedures for detecting the activity of various types of ion transporter in these cells were by monitoring changes in pH_i following various challenges which have been presented earlier (Taylor, 2006; Nicola et al., 2008). Na^+/H^+ exchange can be assayed from the rate of recovery of pH_i after an acid challenge imposed by transient exposure to NH_4Cl for cells in nominally bicarbonate-free medium. Cl^-/HCO_3^- exchange can be assayed with cells in bicarbonate-buffered medium by the rate of alkalinization observed when external Cl^- is removed. Na^+/H^+ exchange in RBECs has been shown to be inhibited by EIPA with an IC_{50} near 0.5 μM (Taylor, 2006). Inhibition of this exchange by cariporide in the GPNT cells is shown in Fig. 5 where the IC_{50} is of the order of 1 μM. These results are consistent with transport via NHE1. Cl^-/HCO_3^- exchange in the RBECs was inhibited by DIDS and was not affected by replacement of external Na^+ using $NMDG^+$ (Taylor, 2006). Similar alkalinizations were observed in GPNT

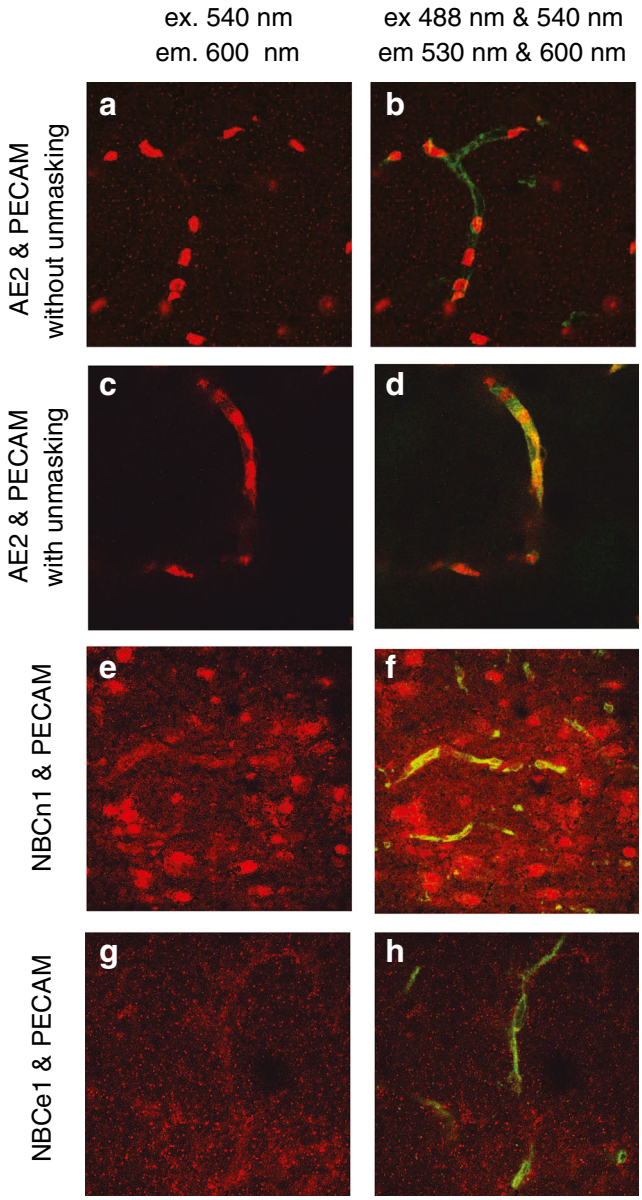

Fig. 2 Confocal images of dual immunofluorescence staining for AE2 or NBCe1 or NBCn1 together with PECAM in thick sections cut from frozen brain segments. Measuring emission at >600 nm (shown as *red*) with excitation only at 540 nm detects only one or another of the transporters. With excitation at both 488 and 540 nM and emission detection at 530±30 nm (shown as *green*) and >600 nm (shown as *red*) PECAM is also detected. The sa6 antibody used in **a**–**d** recognises AE1 present in red blood cells, but after unmasking it also detects AE2 which is seen to outline the vessel with little labelling elsewhere. In **e** and **f**, anti-NBCn1 appears to label the blood vessels. In **g** and **h**, there is a suggestion that anti-NBCe1 labelling also follows the blood vessels. In these two frames, the red channel signal has been multiplied by 1.5. No labelling distinguishable from the general background, which includes staining of other cell types, was observed for anti-NBCe2, anti-NCBE, anti-NDCBE and anti-NHE1 (N1P1 antibody)

cells as can be seen in the controls for the experiments reported in Fig. 7.

Another more specific method for identification of transporters is provided by transfection of siRNA to reduce the

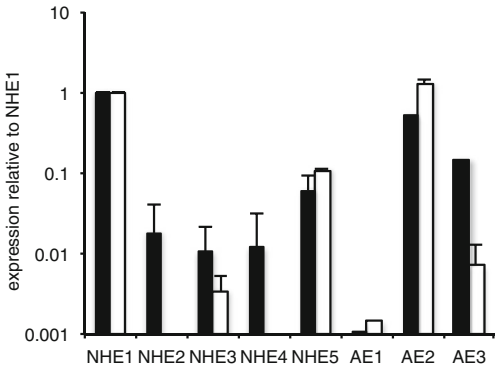

Fig. 3 Expression of NHEs and AEs at mRNA level in cultured rat brain endothelial cells. Expression is shown relative to that for NHE1 in the same cell type. *Black bars* for RBEC primary cultured cells; *open bars* are for the GPNT immortalised cell line. Data are shown as mean ± s.e.m. $n=5$ or 6 except for AE1 RBEC $n=1$, AE1 GPNT $n=1$, AE3 RBEC $n=2$ and AE3 GPNT $n=3$. In the GPNT cells, there was no detectable expression of NHE2 in any experiment (NHE4 was not tested), while for AE1 there was no detectable expression in either RBEC or GPNT cells in two experiments. In GPNT cells, the expression of NHE1 relative to GAPDH was 0.017±0.001, $n=6$

levels of transporter expressed. This technique was applied to both RBECs and GPNT cells but was found to be more effective in the immortalized GPNT cells. Using either of two different siRNA constructs in the GPNT cells, it was possible to reduce the level of mRNA for AE2 by about

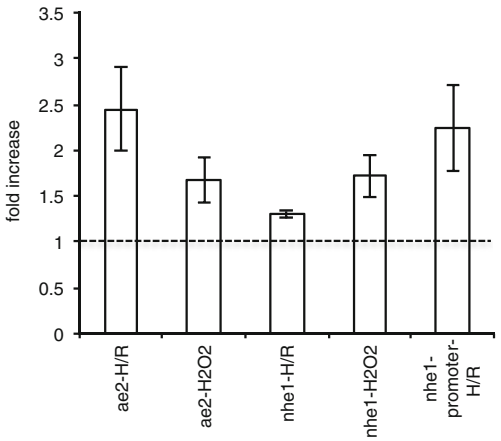

Fig. 4 Effects of hypoxia/reoxygenation or exposure to hydrogen peroxide on expression of NHE1 and AE2 in GPNT cells. The first four *bars* represent fold changes in AE2 or NHE1 mRNA levels and the last bar shows fold change in NHE1 promoter activity relative to paired untreated controls. H/R consisted of hypoxia at 1 % O_2 for 6 h followed by reoxygenation for 24 h. H_2O_2 was applied at 100 μM and left for 6 h. Promoter activity was measured using luciferase reporter gene assay as described in "Methods". For H/R, expression levels were first normalized to those for HPRT under the same conditions, and the ratios were then compared between exposed cells and unexposed controls. For H_2O_2 exposure normalization was to expression of β-actin. These reference genes have been shown previously to vary little with hypoxia/reoxygenation and peroxide exposure, respectively [63]. All ratios shown (mean ± s.e.m.) are significantly different from 1. From *left* to *right*: $n=8$, $p<0.01$; $n=5$, $p<0.05$; $n=4$, $p<0.01$; $n=4$, $p<0.05$; $n=6$, $p<0.05$; *t*-tests for the logs of the ratios compared to zero

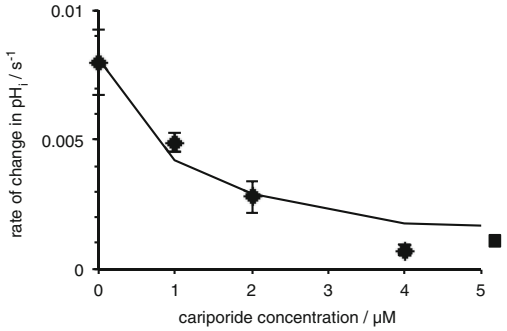

Fig. 5 Inhibitory effect of cariporide on the rate of recovery of intracellular pH (pH_i) after an ammonium pulse in GPNT cells. pH_i was measured using BCECF as described in "Methods". Data are shown as mean ± s.e.m., $n=4$. The *square symbol* to the *right* indicates the rate of change after complete replacement of external Na^+ by $NMDG^+$, which should eliminate all transport via NHEs and is therefore taken as an estimate of the limiting value for pH_i changes in the presence of large cariporide concentrations. The fitted *curve* corresponds to a IC_{50} for cariporide of 1.1 μM. The 95 % confidence limits for the IC_{50} are 0.2 and 2.7 μM

50 %, and using one siRNA construct, similar results were obtained for NHE1 (see Fig. 6). That the reduction was not due to the transfection process itself was demonstrated from the lack of effect of transfection with the "AllStars" construct. (Successful transfection of the fluorescent "AllStars" construct was confirmed by flow cytometry; data not shown.)

Functional assays were undertaken in the transfected GPNT cells with altered NHE1 and AE2 expression, and the results are shown in Fig. 7. Example traces are given in Fig. 7a–f and results are summarized in Fig. 7g, h. The two siRNAs targeted at AE2 each produced a significant reduction in Cl^-/HCO_3^- exchange (Fig. 7g), while the siRNA targeted against NHE1 significantly reduced Na^+/H^+ exchange.

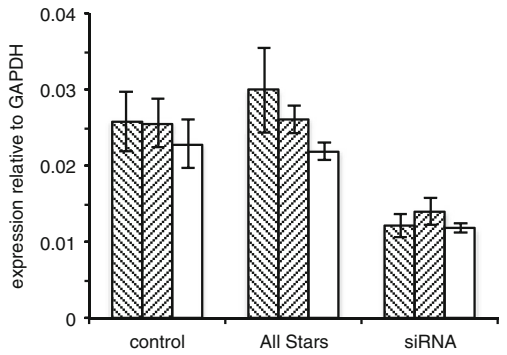

Fig. 6 mRNA levels of AE2 (*hashed bars*) and of NHE1 (*open bars*) in rat brain endothelial GPNT cells following treatment as described in "Methods" without (control) or with either gene specific siRNA (siRNA) or a scrambled sequence ("All Stars"). For AE2, where two different sequences were used, data are given for each set of experiments (represented by the two separate hashed bars). Values shown are the mean ± s.e.m., $n=3$

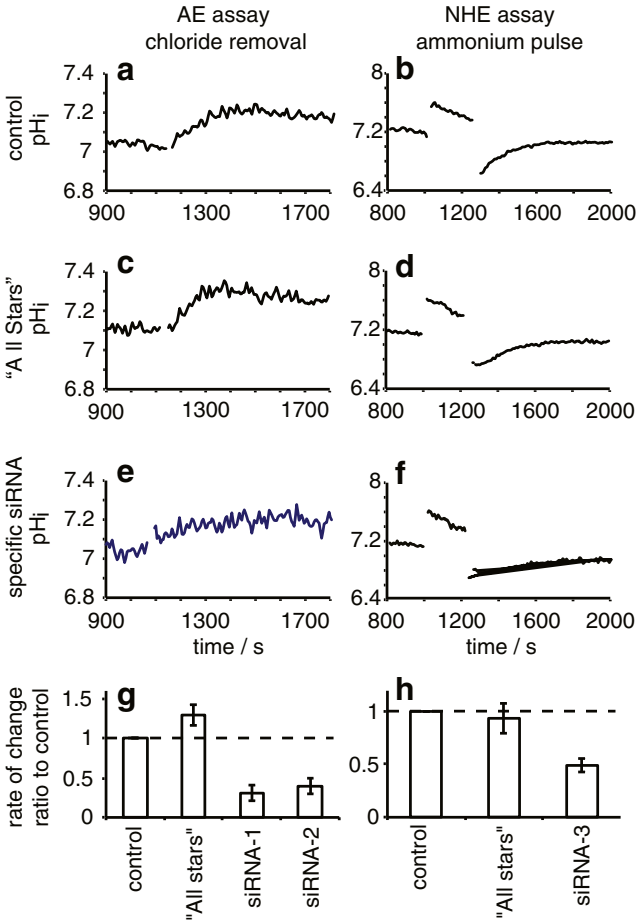

Fig. 7 Functional effects of siRNA targeted against AE2 or NHE1 in GPNT cells. AE function shown in **a**, **c**, **e** and **g** was assessed using the initial rate of increase in intracellular pH induced by removing Cl^- from the extracellular medium. Cells were initially suspended in HCO_3^-- and Cl^--containing medium and after 1,150 s were transferred to medium in which all Cl^- was replaced by gluconate which stimulates HCO_3^- influx in exchange for Cl^- efflux. The initial rate was calculated from the slope of a straight line fitted by eye to the 100 s of the trace after Cl^- removal. NHE function shown in **b**, **d**, **f** and **h** was assessed using the initial rate of increase in intracellular pH in nominally HCO_3^--free medium during recovery after a 200-s exposure to 20 mM NH_4Cl. The initial rate was calculated from an exponential curve fitted to the data by least squares minimization (example shown in **f**). **a**–**f** Examples of traces observed. **a** and **b** show rates observed in cells not transfected with siRNA, **c** and **d** are for cells transfected with "All Stars" siRNA that should have no specific effect on transporter levels, and **e** and **f** are for cells transfected with siRNA-1 specific for AE2 or siRNA-3 specific for NHE1, respectively. Ratios of the rates observed for the transfected cells to those for the corresponding paired controls are shown for AE2 in **g** and for NHE1 in **h**. Data for the "All Stars" transfected cells are not significantly different from control, while those for siRNA-1,2,3 are significantly less ($n=3$, $p<0.05$, 0.05 and 0.01, respectively; *t*-test against 0 for the logarithm of the ratio)

Discussion

Detection of transporters and their functions

To identify ion transporters on brain microvessels, immunohistochemical staining using thin wax-embedded brain

sections was used initially. Such a method has been a key tool in identifying the molecular species responsible for ion transport in specialized epithelia such as kidney and choroid plexus where high-resolution optical images clearly indicate basolateral or apical locations for many of the transporters of interest (see references in Table 1 and [18]). However, these same procedures when used on brain sections (see Fig. 1) were unable to detect any staining on microvessels, the reasons almost certainly being that the lining endothelial cells are very thin, with membranes lacking much folding and that the transporters they express are at lower densities than in specialized epithelia.

To increase the sensitivity of detection, thick frozen sections were used, though this led to some loss of spatial resolution. The positions of the microvessels within the sections were determined by labelling with an antibody to a known endothelial cell marker, PECAM (CD31), together with that to the transporter of interest. This dual-labelling procedure provided clear evidence for AE2 protein along the microvessels (Fig. 2). There was also labelling along microvessels for NBCn1 and NBCe1. For the other transporters investigated (NBCe2, NCBE, NDCBE and NHE1), it was not possible to distinguish staining of microvessels from that of surrounding parenchymal cells. While the methods used here provide evidence for the presence of AE2, NBCn1 and NBCe1 on brain microvessels, they are incapable of localizing these transporters to specific membranes. It is interesting to note that O'Donnell and coworkers [41, 53] had to use immunoelectron microscopy in slices from rat brains to locate NHE1 and NHE2 on luminal and abluminal endothelial cell membranes with 65–75 % and 75–80 %, respectively, being found on the luminal side.

Functional activities of the transporters were investigated using brain endothelial cells in culture. Previous studies on cultured rat brain endothelial cells (RBECs) have detected Na^+, HCO_3^- cotransport, Cl^-/HCO_3^- exchange and Na^+/H^+ exchange [49, 68, 76]. All of these activities were found also in the GPNT-immortalized rat brain endothelial cells, which were used here for transfection studies (see later discussion). There was substantial expression at mRNA level of NBCn1 and NBCe1, the same Na^+, HCO_3^- cotransporters detected at protein level in the brain slices. AE2 was also seen prominently both at mRNA level in the cultured cells and as protein in the slices and could account for the Cl^-/HCO_3^- exchange observed in the cultured cells. NHE1 was seen prominently as mRNA in both the RBEC and GPNT cells, while mRNA for NHE2 was present at about 50-fold lower levels than NHE1 in the RBECs. With RBECs [75], as Lam et al. [41] reported for bovine cortical microvascular endothelial cells, both NHE1 and NHE2 were seen in western blots. As shown previously, the Na^+/H^+ exchange observed in RBECs was inhibitable by EIPA [68, 76, 79]. However, this does not distinguish between the two NHE forms, so for a more precise identification, EIPA was replaced by cariporide in the investigations with GPNT cells (see Fig. 5). IC_{50} values for cariporide acting on NHE1 and NHE2 have been reported by others to be 0.03–3.4 μM and 4.3–62 μM, respectively [44]. The IC_{50} value found here for GPNT cells of 1.1 μM falls clearly within the lower range, consistent with the mRNA observations of NHE1 but not NHE2 in these cells. The value observed for bovine cortical microvascular endothelial cells, 7 μM [41], may indicate both NHE1 and NHE2 to be important in those particular cells.

The use of siRNA to depress levels of mRNA and function in cells provided another means of identifying the molecular species responsible for the activities observed. The effects of two siRNA sequences targeted against AE2 and one against NHE1 were assessed in the GPNT cells. Each of the sequences directed against AE2 significantly depressed both AE2 mRNA expression and the alkalinization resulting from Cl^-/HCO_3^- exchange following the removal of external chloride from HCO_3^--buffered medium. Similarly, the sequence directed against NHE1 significantly depressed both NHE1 mRNA expression and the alkalinization following an imposed acid load seen with nominally HCO_3^--free medium. These data provide evidence that AE2 and NHE1 not only are present but also account at least in part for the activities in GPNT cells as described earlier. However, it remains possible that in RBEC cells where NHE2 is detectable, NHE2 may also contribute.

Experiments were performed to determine whether oxidative challenge might alter not only the expression of AE2 and NHE1 but also the activity of the NHE1 promoter. For this purpose, GPNT cells were used, these being more readily amenable to the necessary transfection. Either direct application of H_2O_2 or exposure of the cells to 6 h of hypoxia, 1 % O_2, followed by 16 h of normoxia significantly increased the expression of mRNA for AE2 and NHE1. Furthermore, using a luciferase reporter gene construct, it was also shown that the activity of the NHE1 promoter was increased by hypoxia/reoxygenation. These observations accord with those of Lam et al. [41] who found increased Na^+/H^+ exchange activity following exposure to hypoxia for 30 min in cortical microvascular endothelial cells. If such changes were to occur in vivo, the greater activities of NHE1 and AE2 would be expected to increase the net transport of Na^+ and HCO_3^- into the brain. This could have implications for ion transport/fluid secretion at the blood–brain barrier following ischaemia (see final section).

A current model of ion transport at the blood–brain barrier

The ion transporters identified in the present study may be inserted into the current model of blood–brain barrier transport as shown in Fig. 8. The primary route for Na^+ entails entry from the blood via NKCC1 [26, 54, 72]; however some

must also enter in conjunction with HCO_3^- transport. Net exit of Na^+ into the brain occurs primarily via Na^+, K^+–ATPases [5, 6, 25, 26, 48, 65], but possibly some Na^+ could exit by cotransport with HCO_3^-. HCO_3^- can enter the cell from the blood directly by one or both of the NBCs identified here, i.e. NBCe1 (in its 2 HCO_3^- to 1 Na^+ mode) or NBCn1. It can also enter indirectly by diffusion of CO_2, its hydration to carbonic acid catalyzed by carbonic anhydrase, dissociation of that to form H^+ and HCO_3^- and transport of the H^+ to the blood via NHE1 and possibly NHE2. Under unchallenged conditions where endothelial cell pH_i is >7, Na^+/H^+ exchange and thus CO_2 hydration are relatively unimportant [49], which can explain the lack of inhibition by acetazolamide (an inhibitor of carbonic anhydrase) of blood–brain barrier secretion observed in vivo (see page 739 in [21]). When pH_i is reduced, as occurs under ischaemic conditions, Na^+/H^+ exchange then becomes important [49], and as shown here NHE1 mediates at least part of this activity. Net exit of HCO_3^- into the brain may occur via Cl^-/HCO_3^- exchange mediated by AE2 and possibly via NBCe1 (in 1 Na^+/3 HCO_3^- mode as in renal proximal tubules [64, 70, 83] and as shown for NBCe2 in choroid plexus [18]).

Cl^- enters the endothelial cells from the blood via NKCC1 and, if internal Cl^- is less than about 95 mM, will also enter the cells via AE2. It may leave into the brain by as yet unidentified Cl^- channels or K^+, Cl^- cotransporters. A volume-activated Cl^- channel has been found in these cells [80], which, though unlikely to be the route for Cl^- exit in the absence of cell swelling, may be important in Cl^- transport during ischaemia. More Cl^- enters cells across the luminal membrane via NKCC1 than is transported across to the brain, so at least some must exit on the luminal side. Thus, there must be an as yet unidentified route for Cl^- to leave cells on the blood side and again the suggested routes are channels and K^+, Cl^- cotransporters.

As indicated in Fig. 8, K^+ can enter via NKCC1 on the luminal side and via the Na^+ pump on the abluminal side [26], in both cases in much larger amounts than are transported across the endothelium. Thus, there must be routes for K^+ recycling across both membranes [47], which could be K^+ channels, some of which are known to be present,[2] or possibly K^+ , Cl^- cotransporters. The presence of passive transport routes for K^+ in both membranes is consistent with observations that the K^+ permeability of the blood–brain barrier in vivo is ca. tenfold higher than the permeability to Na^+ or Cl^- [22, 69].[3]

The importance of blood–brain barrier ion transport

Under normal conditions, ion transport and relatively high water permeability across the blood–brain barrier are important in helping to determine the ionic composition and volume of the ISF. The net flow of fluid produced also aids in the removal of high molecular weight blood–brain barrier impermeant materials from the brain. [17].

However, following ischaemia, uptake and release of ions by cells within the brain are also important in determining the composition and volume of the ISF. Within a few minutes of onset of ischaemia, there is generation of non-volatile acid and consequent decrease in both intracellular and ISF pH, net cellular uptake of Na^+ and Cl^- and release of K^+, cell swelling and decreased ISF volume [24, 38, 43, 67, 73]. Nevertheless, for the total volume to increase, i.e. for there to be oedema, the ISF must be replenished by a rate of fluid secretion across the blood–brain barrier that exceeds the rate of fluid loss from the brain [4]. The rate of loss will be reduced from its pre-ischaemic value by the decreased size of interstitial spaces [67], and furthermore the rate of secretion is increased [7, 14].

While continued or increased transport across the blood–brain barrier during ischaemia may be beneficial in countering changes in interstitial K^+ concentration and pH, secretion of Na^+ and Cl^- will contribute to oedema. Thus, in targeting the blood–brain barrier to reduce the effects of ischaemia, it would be desirable to inhibit Na^+ and Cl^- secretion while not impairing or even increasing the transport of K^+ from the brain and the secretion of HCO_3^- into the brain. Of the transport activities now known to exist in the endothelial cells,

[2] There is evidence for several types of K^+ channel in brain endothelial cells, though some is contradictory. Thus, Hoyer et al. [31] found inwardly rectifying K^+ channels on the abluminal membrane, a location well suited to recycling K^+ that entered the cells via Na^+, K^+–ATPase; Millar et al. [47] found both mRNA and functional fingerprints for Kv1 and Kir2 channels but not Ca^{2+}-activated channels; and van Renterghem et al. [78] and Chen et al. [13] found Ca^{2+}-activated channels. The differences may be the result of different experimental conditions for the patch-clamp experiments used to identify the channels. Regardless, the available evidence indicates that there are several possible routes for K^+ efflux from brain endothelial cells.

[3] Despite widespread acceptance of the view that net movement of K^+ across the blood–brain barrier is from brain to blood, see e.g. [52], the direction of this net movement has not been established and may vary. K^+ concentration is less in ISF than in plasma (see [21] for a review); this has been taken as evidence that K^+ must be actively transported from brain to blood across the blood–brain barrier. However, if K^+ is removed from the brain via ISF outflow, then at steady state K^+ concentration within ISF is determined by the ratio of the net rates at which K^+ and volume are *added* to the brain compartment by all other routes to replace materials removed via the outflow. Thus, to achieve a lower ISF K^+ concentration, there is no need that K^+ be transported back to the blood by an active process.

A more subtle argument can be based on the data of Bito and Davson [8] who found that the K^+ concentration of CSF in the cortical subarachnoid spaces, 2.65 ±0.1 mequiv/kg H_2O, is lower than that of CSF in the cisterna magna, 2.98±0.06 mequiv/kg H_2O (data for dogs, with similar results for cats). They took this observation to imply that K^+ was being removed from the CSF by diffusion into the cortical parenchyma as the CSF flowed from the cisterna magna to the subarachnoid spaces. This removal could be sustained at steady state if there were net K^+ transport out of the ISF across the blood–brain barrier. However, again there are alternative explanations. Thus, the CSF K^+ concentration could also be reduced if fluid with a lower K^+ concentration were added to the CSF during passage from cisternae to subarachnoid space.

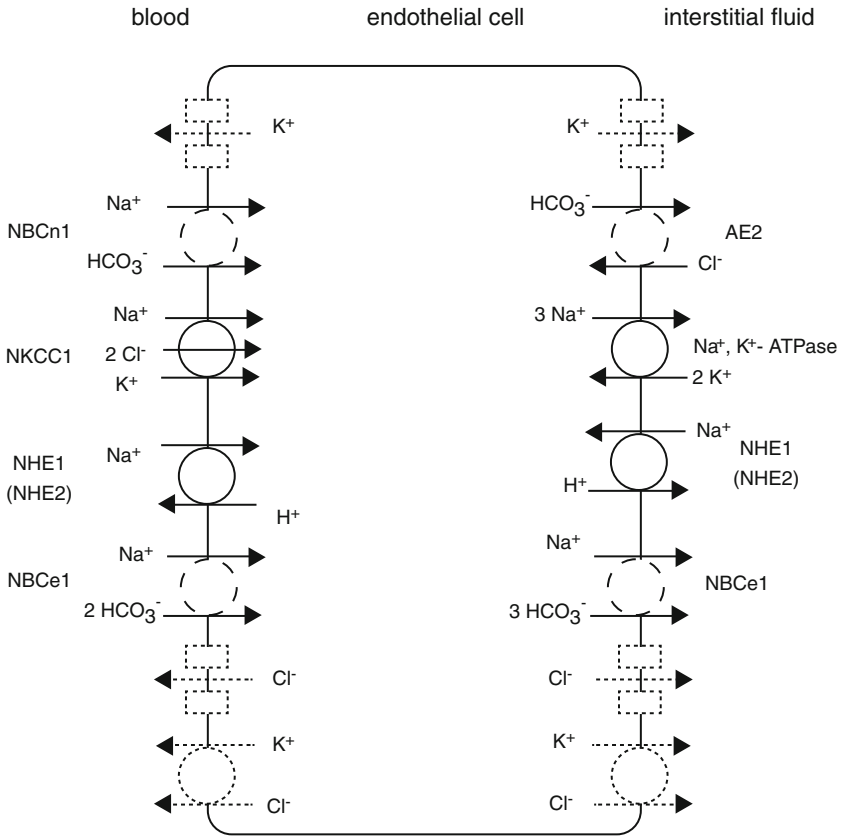

Fig. 8 Schematic diagram of the transporters putatively involved in movement of ions across the blood–brain barrier. Transporters drawn as *solid lines* are already identified and with known locations, those shown as *dashed lines* are already identified but with suggested locations and those drawn as *dotted lines* indicate possible activities in the membranes indicated. Some route/s in addition to those shown solid or dashed must exist in each membrane for each of K^+ and Cl^-. Transporter names are defined in the tables. Transported species are indicated at the source end of each *arrow*. NHE is shown in both membranes [41, 53]

if they were to be distributed as shown in Fig. 8, the most appropriate target for inhibition would be NKCC1. Inhibiting this transporter would reduce the movements of Na^+, K^+ and Cl^- towards the brain without directly impairing secretion of HCO_3^- or removal of H^+. Indeed marked reduction in oedema and infarct size following middle cerebral artery occlusion in the rat has been seen with bumetanide, an inhibitor of NKCC1 [52, 54].

The NHE1 and NHE2 inhibitor, cariporide, has also been shown to reduce oedema and infarct size following middle cerebral artery occlusion [53]. If its action is on secretion across the blood–brain barrier, then it must be inhibiting, directly or indirectly, both Na^+ and Cl^- movements towards the brain. Such inhibition would occur if both the Na^+/H^+ exchanger, NHE1 or NHE2, and Cl^-/HCO_3^- exchanger, AE2, were located in the luminal membrane of the endothelial cells as suggested by O'Donnell [52]. Direct NHE inhibition would lead to a decrease in intracellular pH and HCO_3^- concentration, which would in turn reduce Cl^-/HCO_3^- exchange, with the net effect of reducing NaCl entry across the luminal membrane. However, while placing AE2 in the luminal membrane is consistent with the data for Cl^-/HCO_3^- exchange in cultured brain endothelial cells [49, 76], it is not consistent with the proposed role for AE2 in normal secretion across the blood–brain barrier: Cl^-/HCO_3^- exchange across the luminal membrane would oppose the net secretion of HCO_3^-. There are several possible resolutions of this inconsistency: a mechanism other than Cl^-/HCO_3^- exchange by AE2 accounts for either entry of Cl^- to the cells during ischaemia or exit of HCO_3^- in normal secretion[4]; AE2 may relocate from abluminal to luminal membranes during ischaemia; cariporide may not be having its effects via inhibition of NHE in the endothelium but rather by inhibition of NHE in cells within the brain parenchyma. This last option is also pertinent to interpretation of the in vivo effects of bumetanide as discussed earlier.

NKCC1 and the NHEs are known to be present on neurons and astrocytes within the brain parenchyma. If inhibitors of these transporters reach the parenchyma, they will produce marked reductions in the responses of the parenchymal cells to ischaemia with less cellular uptake of Na^+ and Cl^-, less release of K^+, reduced cell swelling [12, 36, 56, 71, 81, 82] and presumably also less contraction of the interstitial spaces. These inhibitor effects within the parenchyma may have consequences quite independently of any direct effects of the inhibitors on the endothelial cells that counter changes in the rates of blood–brain barrier secretion and ISF loss to CSF seen

[4] It has already been noted that there must be on the luminal membrane at least one unidentified route, which cannot be AE2, to allow recycling of a portion of the Cl^- that enters via NKCC1. Similarly, there may be alternatives to AE2 for the HCO_3^- efflux to the brain.

without the inhibitors (see e.g. [66, 67]). Whether or not the inhibitors reach sites within the parenchyma in sufficient concentrations is at present unknown,[5] and it is prudent to regard the reductions in the extent of oedema and infarct volume as results of effects on both the endothelial cells and parenchymal cells. The relative importance of these sites of action may be different for bumetanide and cariporide.

In summary, results of the current study identify AE2, NBCn1 and NBCe1 on microvessels in the brain. Experiments on endothelial cells in culture demonstrate that these transporters can make a substantial contribution to movement of ions into and out of the endothelium. Further work is now required to determine the localization of these bicarbonate transporters to luminal or abluminal membranes of the endothelial cells as noted by O'Donnell [52] as well as to identify and localize additional transport mechanisms that must exist for K^+ and Cl^-.

Acknowledgments We acknowledge with thanks that Kasia Kania supplied the construct for detecting NHE1 promoter activity and helped carry out the experiments using it, Seth Alper provided generous supplies of the anti-AE2 antibody, Jeppe Praetorius hosted CJT in Aarhus for the thin section studies and supplied many of the antibodies used in these and the thick section studies in Cambridge (see Tables 1 and 2), Josette Noel provided the n1p1 antibody; and Juergen Puenter (Sanofi-Aventis Deutschland GmbH) provided the cariporide. The early stages of this work were supported by BBSRC grant No. S19517, late stages by grants from the Department of Pharmacology. RM was supported by a Gates Fellowship. SW was sponsored by the Cambridge Overseas Trust.

All experiments were performed in compliance with the current laws of the country in which they were performed. The authors declare that they have no conflicts of interest.

[5] Bumetanide is a carboxylic weak acid that will be present primarily in anionic form at pH 7.4, while cariporide, pKa 6.28 [44], is a weak base present primarily in neutral form. Both are absorbed well from oral doses, and thus they succeed in crossing the epithelial cells of the gut wall. For bumetanide, in the rat, concentrations have been measured simultaneously in blood and brain following single doses. The earlier of two studies reports bumetanide concentration in brain to be increasing over an hour [10], while the later finds that the concentrations in both serum and brain increase to a peak at half an hour and then fall by more than 75 % over the next half hour [42]. Both find that bumetanide enters brain tissue but to different extents and with different kinetics. In the rat, approximately 98 % of bumetanide in plasma is bound to plasma proteins [39]. Thus, total concentrations in the brain as small as 2 % of those in plasma might reflect either slow penetration across the blood–brain barrier or a lack of binding in brain tissue or both. Low concentrations with rapid removal from the brain [42] would imply little binding and rapid penetration. No data for penetration of cariporide into cells or across the blood–brain barrier appear to have been published [23]. However, it is a small molecule, MW 284, with a neutral form that is known to cross cell membranes in the gut. As a weak base, it might even be a candidate for weak base trapping in ischaemic regions of low pH within the brain parenchyma.

References

1. Abbott NJ (2004) Evidence for bulk flow of brain interstitial fluid: significance for physiology and pathology. Neurochem Int 45:545–552
2. Alper SL, StuartTilley AK, Biemesderfer D, Shmukler BE, Brown D (1997) Immunolocalization of AE2 anion exchanger in rat kidney. Am J Physiol 42:F601–F614
3. Barrand MA, Robertson KJ, von Weikersthal SF (1995) Comparisons of P-glycoprotein expression in isolated rat brain microvessels and in primary cultures of endothelial cells derived from microvasculature of rat brain, epididymal fat pad and from aorta. FEBS Lett 374:179–183
4. Betz AL, Ennis SR, Schielke GP (1989) Blood–brain barrier sodium transport limits development of brain edema during partial ischemia in gerbils. Stroke 20:1253–1259
5. Betz AL, Firth JA, Goldstein GW (1980) Polarity of the blood–brain barrier: distribution of enzymes between the luminal and antiluminal membranes of brain capillary endothelial cells HCO_3^-. Brain Res 192:17–28
6. Betz AL, Goldstein GW (1980) The basis for active transport at the blood–brain barrier. Adv Exp Med Biol 131:5–16
7. Betz AL, Keep RF, Beer ME, Ren XD (1994) Blood–brain-barrier permeability and brain concentration of sodium, potassium, and chloride during focal ischemia. J Cereb Blood Flow Metab 14:29–37
8. Bito LZ, Davson H (1966) Local variations in cerebrospinal fluid composition and its relationship to the composition of the extracellular fluid of the cortex. Exp Neurol 14:264–280
9. Bouzinova EV, Praetorius J, Virkki LV, Nielsen S, Boron WF, Aalkjaer C (2005) Na+-dependent HCO_3^- uptake into the rat choroid plexus epithelium is partially DIDS sensitive. Am J Physiol 289: C1448–C1456
10. Brandt C, Nozadze M, Heuchert N, Rattka M, Loscher W (2010) Disease-modifying effects of phenobarbital and the NKCC1 inhibitor bumetanide in the pilocarpine model of temporal lobe epilepsy. J Neurosci 30:8602–8612
11. Brown D, Lydon J, McLaughin M, StuartTilley A, Tyszkowski R, Alper S (1996) Antigen retrieval in cryostat tissue sections and cultured cells by treatment with sodium dodecyl sulfate (SDS). Histochem Cell Biol 105:261–267
12. Chen H, Luo J, Kintner DB, Shull GE, Sun D (2005) Na(+)-dependent chloride transporter (NKCC1)-null mice exhibit less gray and white matter damage after focal cerebral ischemia. J Cereb Blood Flow Metab 25:54–66
13. Chen Y-J, Yuen N, Wallace BK, Wulff H, O'Donnell ME (2012) Inhibition of the calcium-activated Kca3.1 channel reduces Na plus accumulation and edema formation in the early stages of ischemic stroke. J Vasc Res 49:12–12
14. Chen YJ, Lam TI, Anderson SE, Walton JH, O'Donnell ME (2009) Blood–brain barrier Na-K-Cl cotransporter and Na/H exchanger: therapeutic targets for ischemia-induced brain Na uptake and edema formation. J Cereb Blood Flow Metab 29: S489–S489
15. Cserr HF (1984) Convection of brain interstitial fluid in hydrocephalus. In: Shapiro K, Marmarou A, Portnoy H (eds) Hydrocephalus. Raven, New York

16. Cserr HF, Cooper DN, Milhorat TH (1977) Flow of cerebral interstitial fluid as indicated by removal of extracellular markers from rat caudate-nucleus. Exp Eye Res 25:461–473
17. Cserr HF, Patlak CS (1992) Secretion and bulk flow of interstitial fluid. In: Bradbury MWB (ed) Physiology and Pharmacology of the Blood–brain Barrier. Springer-Verlag, Berlin, pp 245–261
18. Damkier HH, Brown PD, Praetorius J (2010) Epithelial pathways in choroid plexus electrolyte transport. Physiology 25:239–249
19. Damkier HH, Nielsen S, Praetorius J (2006) An anti-NH2-terminal antibody localizes NBCn1 to heart endothelia and skeletal and vascular smooth muscle cells. Am J Physiol 290:H172–H180
20. Damkier HH, Nielsen S, Praetorius J (2007) Molecular expression of SLC4-derived Na+-dependent anion transporters in selected human tissues. Am J Physiol 293:R2136–R2146
21. Davson H, Segal MB (1996) Physiology of the CSF and Blood–brain Barriers. CRC, Boca Raton
22. Davson H, Welch K (1971) The permeation of several materials into the fluids of the rabbit's brain. J Physiol (Lond) 218:337–351
23. Dhein S, Salameh A (1999) Na+/H+-exchange inhibition by cariporide (Hoe 642): a new principle in cardiovascular medicine. Cardiovasc Drug Rev 17:134–146
24. Drewes LR, Gilboe DD (1973) Glycolysis and the permeation of glucose and lactate in the isolated, perfused dog brain during anoxia and postanoxic recovery. J Biol Chem 248:2489–2496
25. Firth JA (1977) Cytochemical localization of the K^+ regulation interface between blood and brain. Experientia 33:1093–1094
26. Foroutan S, Brillault J, Forbush B, O'Donnell ME (2005) Moderate-to-severe ischemic conditions increase activity and phosphorylation of the cerebral microvascular endothelial cell Na+–K+–Cl− cotransporter. Am J Physiol 289:C1492–C1501
27. Ghandour MS, Langley OK, Zhu XL, Waheed A, Sly WS (1992) Carbonic anhydrase-IV on brain capillary endothelial-cells—a marker associated with the blood–brain-barrier. Proc Natl Acad Sci U S A 89:6823–6827
28. Granger D, Marsolais M, Burry J, Laprade R (2003) Na+/H+ exchangers in the human eccrine sweat duct. Am J Physiol 285:C1047–C1058
29. Greenwood J, Pryce G, Devine L, Male DK, dosSantos WLC, Calder VL, Adamson P (1996) SV40 large T immortalised cell lines of the rat blood–brain and blood–retinal barriers retain their phenotypic and immunological characteristics. J Neuroimmunol 71:51–63
30. Hadaczek P, Yamashita Y, Mirek H, Tamas L, Bohn MC, Noble C, Park JW, Bankiewicz K (2006) The "perivascular pump" driven by arterial pulsation is a powerful mechanism for the distribution of therapeutic molecules within the brain. Mol Ther 14:69–78
31. Hoyer J, Popp R, Meyer J, Galla HJ, Gogelein H (1991) Angiotensin-II, vasopressin and GTP gamma-S inhibit inward-rectifying-K+ channels in porcine cerebral capillary endothelial-cells. J Membr Biol 123:55–62
32. Iliff JJ, Lee H, Yu M, Feng T, Logan J, Nedergaard M, Benveniste H (2013) Brain-wide pathway for waste clearance captured by contrast-enhanced MRI. J Clin Invest 123:1299–1309
33. Iliff JJ, Wang M, Liao Y, Plogg BA, Peng W, Gundersen GA, Benveniste H, Vates GE, Deane R, Goldman SA, Nagelhus EA, Nedergaard M (2012) A paravascular pathway facilitates CSF flow through the brain parenchyma and the clearance of interstitial solutes, including amyloid beta. Sci Transl Med 4:147ra111
34. Jaulmes A, Thierry S, Janvier B, Raymondjean M, Marechal V (2006) Activation of sPLA2-IIA and PGE2 production by high mobility group protein B1 in vascular smooth muscle cells sensitized by IL-1beta. FASEB J 20:1727–1729
35. Jensen LJ, Stuart-Tilley AK, Peters LL, Lux SE, Alper SL, Breton S (1999) Immunolocalization of AE2 anion exchanger in rat and mouse epididymis. Biol Reprod 61:973–980
36. Kahle KT, Simard JM, Staley KJ, Nahed BV, Jones PS, Sun D (2009) Molecular mechanisms of ischemic cerebral edema: role of electroneutral ion transport. Physiology 24:257–265
37. Kashgarian M, Biemesderfer D, Caplan M, Forbush B 3rd (1985) Monoclonal antibody to Na, K–ATPase: immunocytochemical localization along nephron segments. Kidney Int 28:899–913
38. Katsura K, Kristian T, Siesjo BK (1994) Energy metabolism, ion homeostasis, and cell damage in the brain. Biochem Soc Trans 22:991–996
39. Kim EJ, Lee MG (2001) Pharmacokinetics and pharmacodynamics of intravenous bumetanide in mutant Nagase analbuminemic rats: importance of globulin binding for the pharmacodynamic effects. Biopharm Drug Dispos 22:147–156
40. Kwon TH, Fulton C, Wang WD, Kurtz I, Frokiaer J, Aalkjaer C, Nielsen S (2002) Chronic metabolic acidosis upregulates rat kidney Na– HCO_3^-cotransporters NBCn1 and NBC3 but not NBC1. Am J Physiol 282:F341–F351
41. Lam TI, Wise PM, O'Donnell ME (2009) Cerebral microvascular endothelial cell Na/H exchange: evidence for the presence of NHE1 and NHE2 isoforms and regulation by arginine vasopressin. Am J Physiol 297:C278–C289
42. Li Y, Cleary R, Kellogg M, Soul JS, Berry GT, Jensen FE (2011) Sensitive isotope dilution liquid chromatography/tandem mass spectrometry method for quantitative analysis of bumetanide in serum and brain tissue. J Chromatogr B Anal Technol Biomed Life Sci 879: 998–1002
43. Lundbaek JA, Hansen AJ (1992) Brain interstitial volume fraction and tortuosity in anoxia. Evaluation of the ion-selective microelectrode method. Acta Physiol Scand 146:473–484
44. Masereel B, Pochet L, Laeckmann D (2003) An overview of inhibitors of Na+/H+ exchanger. Eur J Med Chem 38:547–554
45. Maunsbach AB, Vorum H, Kwon TH, Nielsen S, Simonsen B, Choi I, Schmitt BM, Boron WF, Aalkjaer C (2000) Immunoelectron microscopic localization of the electrogenic Na/HCO2 cotransporter in rat and ambystoma kidney. J Am Soc Nephrol 11:2179–2189
46. Milhorat TH, Hammock MK, Fenstermacher JD, Rall DP, Levin VA (1971) Cerebrospinal fluid production by the choroid plexus and brain. Science 173:330–332
47. Millar ID, Wang S, Brown PD, Barrand MA, Hladky SB (2008) Kv1 and Kir2 potassium channels are expressed in rat brain endothelial cells. Pflügers Arch 456:379–391
48. Nag S (2003) Ultracytochemical studies of the compromised blood–brain barrier. In: Nag S (ed) The Blood–brain Barrier. Biology and Research Protocols. Humana, Totowa, pp 145–160
49. Nicola PA, Taylor CJ, Wang S, Barrand MA, Hladky SB (2008) Transport activities involved in intracellular pH recovery following acid and alkali challenges in rat brain microvascular endothelial cells. Pflügers Arch 456:801–812
50. Nielsen S, Nagelhus EA, AmiryMoghaddam M, Bourque C, Agre P, Ottersen OP (1997) Specialized membrane domains for water transport in glial cells: high-resolution immunogold cytochemistry of aquaporin-4 in rat brain. J Neurosci 17:171–180
51. Nielsen S, Smith BL, Christensen EI, Knepper MA, Agre P (1993) CHIP28 water channels are localized in constitutively water-permeable segments of the nephron. J Cell Biol 120:371–383
52. O'Donnell ME (2009) Ion and water transport across the blood–brain barrier. In: Alvarez-Leefmans FJ, Delpire E (eds) Physiology and Pathology of Chloride Transporters and Channels in the Nervous System: from Molecules to Diseases. Elsevier Science, Amsterdam, pp 585–606
53. O'Donnell ME, Chen YJ, Lam TI, Taylor KC, Walton JH, Anderson SE (2013) Intravenous HOE-642 reduces brain edema and Na uptake in the rat permanent middle cerebral artery occlusion model of stroke: evidence for participation of the blood–brain barrier Na/H exchanger. J Cereb Blood Flow Metab 33:225–234

54. O'Donnell ME, Tran L, Lam TI, Liu XB, Anderson SE (2004) Bumetanide inhibition of the blood–brain barrier Na–K–Cl cotransporter reduces edema formation in the rat middle cerebral artery occlusion model of stroke. J Cereb Blood Flow Metab 24: 1046–1056
55. Patlak CS, Fenstermacher JD (1975) Measurements of dog blood–brain transfer constants by ventriculocisternal perfusion. Am J Physiol 229:877–884
56. Pedersen SF, O'Donnell ME, Anderson SE, Cala PM (2006) Physiology and pathophysiology of Na+/H+ exchange and Na+–K+–2Cl(−) cotransport in the heart, brain, and blood. Am J Physiol 291: R1–R25
57. Pollay M, Curl F (1967) Secretion of cerebrospinal fluid by the ventricular ependyma of the rabbit. Am J Physiol 213:1031–1038
58. Praetorius J, Nejsum LN, Nielsen S (2004) A SCL4A10 gene product maps selectively to the basolateral plasma membrane of choroid plexus epithelial cells. Am J Physiol 286:C601–C610
59. Praetorius J, Nielsen S (2006) Distribution of sodium transporters and aquaporin-1 in the human choroid plexus. Am J Physiol 291:C59–C67
60. Pushkin A, Clark I, Kwon TH, Nielsen S, Kurtz I (2000) Immunolocalization of NBC3 and NHE3 in the rat epididymis: colocalization of NBC3 and the vacuolar H+–ATPase. J Androl 21: 708–720
61. Pushkin A, Yip KP, Clark I, Abuladze N, Kwon TH, Tsuruoka S, Schwartz GJ, Nielsen S, Kurtz I (1999) NBC3 expression in rabbit collecting duct: colocalization with vacuolar H+–ATPase. Am J Physiol 277:F974–F981
62. Regina A, Romero IA, Greenwood J, Adamson P, Bourre JM, Couraud PO, Roux F (1999) Dexamethasone regulation of P-glycoprotein activity in an immortalized rat brain endothelial cell line, GPNT. J Neurochem 73:1954–1963
63. Robertson SJ, Kania KD, Hladky SB, Barrand MA (2009) P-glycoprotein expression in immortalised rat brain endothelial cells: comparisons following exogenously applied hydrogen peroxide and after hypoxia-reoxygenation. J Neurochem 111:132–141
64. Romero MF, Fong PY, Berger UV, Hediger MA, Boron WF (1998) Cloning and functional expression of rNBC, an electrogenic Na+–HCO_3^- cotransporter from rat kidney. Am J Physiol 274(43):F425–F432
65. Sanchez del Pino MM, Hawkins RA, Peterson DR (1995) Biochemical discrimination between luminal and abluminal enzyme and transport activities of the blood–brain-barrier. J Biol Chem 270: 14907–14912
66. Schielke GP, Moises HC, Betz AL (1990) Potassium activation of the Na, K-pump in isolated brain microvessels and synaptosomes. Brain Res 524:291–296
67. Schielke GP, Moises HC, Betz AL (1991) Blood to brain sodium transport and interstitial fluid potassium concentration during early focal ischemia in the rat. J Cereb Blood Flow Metab 11:466–471
68. Sipos I, Torocsik B, Tretter L, Adam-Vizi V (2005) Impaired regulation of pH homeostasis by oxidative stress in rat brain capillary endothelial cells. Cell Mol Neurobiol 25:141–151
69. Smith QR, Rapoport SI (1986) Cerebrovascular permeability coefficients to sodium, potassium, and chloride. J Neurochem 46:1732–1742
70. Soleimani M, Grassi SM, Aronson PS (1987) Stoichiometry of Na+–HCO_3^- cotransport in basolateral membrane vesicles isolated from rabbit renal cortex. J Clin Invest 79:1276–1280
71. Sun D, Kintner DB, Pond BB (2009) The role of cation-chloride transporters in brain ischemia. In: Alvarez-Leefmans FJ, Delpire E (eds) Physiology and Pathology of Chloride Transporters and Channels in the Nervous System: from Molecules to Diseases. Elsevier Science, Amsterdam, pp 501–517
72. Sun D, Lytle C, O'Donnell ME (1995) Astroglial cell-induced expression of Na–K–Cl cotransporter in brain microvascular endothelial cells. Am J Physiol 269:C1506–C1512
73. Sykova E, Nicholson C (2008) Diffusion in brain extracellular space. Physiol Rev 88:1277–1340
74. Szentistvanyi I, Patlak CS, Ellis RA, Cserr HF (1984) Drainage of interstitial fluid from different regions of rat brain. Am J Physiol 246: F835–F844
75. Taylor CJ (2004) Intracellular pH regulation in rat brain endothelial cells. Department of Pharmacology, Ph.D. dissertation, University of Cambridge, Cambridge
76. Taylor CJ, Nicola PA, Wang S, Barrand MA, Hladky SB (2006) Transporters involved in the regulation of intracellular pH (pHi) in primary cultured rat brain endothelial cells. J Physiol (Lond) 576: 769–785
77. Terris J, Ecelbarger CA, Marples D, Knepper MA, Nielsen S (1995) Distribution of aquaporin-4 water channel expression within rat kidney. Am J Physiol 269:F775–F785
78. Van Renterghem C, Vigne P, Frelin C (1995) A charybdotoxin-sensitive, Ca2+-activated K+ channel with inward, rectifying properties in brain microvascular endothelial-cells—properties and activation by endothelins. J Neurochem 65:1274–1281
79. Vigne P, Ladoux A, Frelin C (1991) Endothelins activate Na+/H+ exchange in brain capillary endothelial cells via a high affinity endothelin-3 receptor that is not coupled to phospholipase C. J Biol Chem 266:5925–5928
80. von Weikersthal SF, Barrand MA, Hladky SB (1999) Functional and molecular characterization of a volume-sensitive chloride current in rat brain endothelial cells. J Physiol (Lond) 516:75–84
81. Walcott BP, Kahle KT, Simard JM (2012) Novel treatment targets for cerebral edema. Neurotherapeutics 9:65–72
82. Yan YP, Dempsey RJ, Flemmer A, Forbush B, Sun DD (2003) Inhibition of Na+–K+–Cl− cotransporter during focal cerebral ischemia decreases edema and neuronal damage. Brain Res 961:22–31
83. Yoshitomi K, Burckhardt BC, Fromter E (1985) Rheogenic sodium-bicarbonate cotransport in the peritubular cell membrane of rat renal proximal tubule. Pflügers Arch 405:360–366